SSRG International Journal of Electrical and Electronics Engineering
ISSN: 2348-8379/ https://doi.org/10.14445/23488379/IJEEE-V10I9P113

Volume 10 Issue 9, 137-153, September 2023

Original Article

Machine Learning Based Electrical Vehicle Charging Management under the Optimization of Flyback Converter for Solar Photovoltaic Applications

P. Dhanalakshmi[1], U. Janardhan Reddy[2], M. Ranjit Reddy[3], G. Ravikanth[4]

[1]*Department of Computer Science & Engineering,*
Mohan Babu University (Erstwhile Sree Vidyanikethan Engineering College), Tirupati, India.
[2]*Department of Computer Science & Engineering, Gitam University, Bengaluru, Karnataka, India.*
[3]*Department of Computer Science & Engineering, Srinivasa Ramanujan Institute of Technology (Autonomous), India.*
[4]*Department of Computer Science & Engineering, BVC College of Engineering (Autonomous), Andhra Pradesh, India.*

[1]*Corresponding Author : mallidhana5@gmail.com*

Received: 17 July 2023 Revised: 21 August 2023 Accepted: 14 September 2023 Published: 30 September 2023

Abstract *- Flyback topologies are an exciting study area for photovoltaic applications driven by their efficiency and low complexity. However, the current converter design has its disadvantages of being heavy and inefficient. However, solar Photovoltaic (PV) systems rapidly expand and hold great promise as a sustainable energy option. Because the converter needs a higher voltage than the PV panels can produce, it is common practice to employ a conversion device. The panel's Maximum Power Point (MPP) has been tracked using the "Perturb and Observe" (P&O) technique. Given that the maximum power output of each converter is only 2/N of the total, the buck converter's power capacity can be significantly increased using N-overlapped flyback converters. To design an optimization strategy for cutting down on power loss within a budgetary constraint, we provide a Model Predictive Control (MPC) MPPT technique. The control loop is reduced in length by using the proposed predictive controller for MPP, which begins to predict errors as soon as the flyback DC/DC converter receives the signal from the switch. Calculating the battery's SoC for an electric car is time-consuming and challenging. This study introduces a machine learning-based technique to better manage energy production in remotely controlled and partitioned solar power plants. The suggested method employs a state-of-the-art support vector machine to model and estimate Hybrid Electric Vehicle (HEV) charging demand. Experimental findings with the integrated circuits are presented and analyzed with mathematical operations, specifications, predictions, and simulators of the power circuits portion of the MPPT converter. Effective clamps are added to the circuit to improve performance under test conditions. The efficiency of the flyback converter with the suggested dynamic resistor divider and the concurrent systems is computationally confirmed using a 250W interleaved flyback converter circuitry setup. Regarding PV panels, sustaining a high voltage and generating substantial electricity production, MPPT is significant. Therefore, it is essential to have an endless energy supply, and it is also crucial to reach self-sufficiency in energy demands. The electrical vehicle load of an ensemble can be partially met by its solar system.*

Keywords *- MPPT, MPC, Photovoltaic system, Solar Energy, MPP, Flyback converter.*

1. Introduction

Usually, a transformer with a low energizing capacitance vs. power is used in flyback converters. However, when the input voltage range is wide, a crucial drawback to utilizing such a transformer is that high equilibrium energy is required. There are either many turns or a low attracted induction value, indicating inefficiency [1]. The greater attracting resistance in the neutral situation may be responsible for an increase in converter efficiency. To use DC-to-DC converters or regulators with high switching frequencies, Switched Mode Power Supply (SMPS) circuits frequently require a high-frequency paired capacitor [2].

Benefits of using AC mains-derived supply include proper voltage scaling and natural isolation after performing the requisite rectifications and filters. The standard input electrical control in a flyback converter operating in Continuous Conduction Mode (CCM) mode is the primary source of complication [3-4].

Recent research efforts have concentrated on evaluating converter losses and improving efficiency. The objective of this study deviates a little from the trends previously identified in that it is more focused on creating a mathematical model of the converter in terms of its parameters [5] rather than

improving the converter itself. The principal voltage divider and clamp circuits without additional circuitry are the subject of this research to increase the power converter's output and efficiency. Due to its negligible adverse effects on the environment, limitless supply, and absence of gathering costs, solar energy has quickly ascended to the top of the renewable energy food chain [6]. So many scientists are making strides in developing uses for solar PV modules beyond only energy generating and water pumping. Since a solar PV system will be used as a source of electricity, a proper maximum power point tracking technique must be implemented [7].

Researchers are making great efforts to find applications for solar PV modules other than energy generation and water pumping. A suitable maximum power point tracking technique must be used because a solar PV system will be used as the power source. When choosing a DC-DC converter, considering the most power points possible dramatically improves the likelihood of a successful implementation. The Sequencing and Resilient Process and the Perturb and Observe Algorithm are two of the most prevalent examples. The P&O is practical but wastes much energy because it repeatedly wanders away from and returns to its maximum power level [8-9].

Furthermore, the P&O algorithm can become jumbled when temperatures and insolation swing dramatically. This method establishes the maximum power point of the PV panel using the direct and periodic conductance connection [10]. Consequently, the technique works even when the temperature and insolation of the surrounding environment change suddenly. However, its reaction is limited because it necessitates intricate calculations to find the maximum power point [11].

These strategies were widely used before MPP because they could maximize power despite abrupt environmental changes. These techniques require a lot of processing power, which makes them difficult and expensive [12]. To balance effectiveness and simplicity, a non-linear controller, such as a sliding mode controller, is provided in the present investigation. This development method can use any Variable Structure System (VSS). PV networks that track the maximum power point in sliding mode instruct the duty cycle to follow peak power output [13].

MATLAB/PC controls the converter's DC power supply, DC load, and switching frequency while measuring input/output power during efficiency characterization. The switching time instruction and the order to turn on or off the valley switching from MATLAB are first sent to the digital controller [14]. The software is then informed of the regulation, on-time, and DCM/CCM status. Additionally, synchronous rectifiers may be utilized in place of diodes in low-output voltage situations to lower primary conduction loss [15].

2. Literature Review

A critical step toward the electrification of cars, using an Electric Motor/Generator (EM) in an EV improves the engine's efficiency. Supervisory control is the vehicle's brain, deciding how the engine, EM, and battery should operate. It consequently significantly impacts how efficient EVs are [16]. SVM in ML learns about the world by trying different actions and gathering state and reward information from the environment. In a series EV, the supervisory activities include dividing the power between the EM and the machine in terms of torque. Still, in a parallel EV, the supervisory measures include separating the power between the engine and EM [17]. Standard metrics include state-of-charge, energy, speed, and acceleration. Although ML-based EV monitoring has lately gained popularity, the lengthy learning curve it requires still prevents its general adoption [18].

The current research covers the issues and inefficiencies of Flyback Converter technology for solar photovoltaic applications. Although flyback converters have the potential to be simple and successful, the contemporary design is inefficient. The necessity for additional conversion devices to meet the demand for a higher voltage output than what PV panels can provide is the cause of this inefficiency. There is a knowledge gap because there are no trustworthy optimization strategies for minimizing power loss within restricted financial limitations.

The investigation draws attention to a significant issue with solar energy plants' management of EV charging. Making a precise estimate of the State of Charge (SoC) battery pack used in an electric car requires much time and effort. Closing this gap requires a more efficient and precise method of regulating EV charging demands in solar-powered systems to promote sustainability and self-sufficiency in energy supply. Research recommends integrating Model Predictive Control (MPC) for MPPT with machine learning-based energy management techniques to solve these gaps. A more sustainable energy future is what the advancements in solar PV system management and flyback converter technology are designed to promote [19-22].

The research being investigated looks into novel ways to make flyback converter designs function better while being smaller and lighter. The power output of the buck converter is considerably increased when N-overlapped flyback converters are used, enabling more efficient energy collection. The overall goal of the inquiry is to attain energy independence, and it accomplishes this by integrating PV systems that can generate a lot of electricity at a steady high voltage. By enhancing power generation and assisting in meeting electric vehicle charging demand, this technique contributes to a more stable and efficient energy ecology. The research's innovation is in its comprehensive, integrated approach to maximizing energy conversion, control, and management in the context of solar PV systems and EV charging, enhancing energy

solutions' efficiency and long-term viability. According to the research [23], this study simulates the DBFI to analyze the electrical degradation dispersion throughout the circuit and look for ways to improve effectiveness. The results demonstrate that a CMS was incorporated into the proposed DBFI to reduce low-order distortions. The study [24] suggested multistage micro-inverter systems for lightweight PV systems that used a separate Neutral Position Clamped (D-NPC) converter. We also offer a micro-inverter built around a D-NPC inverter in this work, and we enhance its functionality to increase its dependability and efficiency [25].

According to the investigation [26], Differential Power Processing (DPP) converters have been suggested to solve the mismatch concerns in conventional flat PV panels. We investigate the reasons behind the solar roof irradiation difference on Prius PHEVs. Then, various DPP converter topologies are compared to select the best DPP converter topology for PHEVs. Following the topology's optimization for PHEV applications, the system's performance is carefully reviewed. Last, we observe the outcomes of testing the prototype inside and outside. Road tests revealed that installing the proposed DPP converter on a Prius PHEV's solar roof increased its daily energy output by 4-5%.

A high-step-up, multistage structure with many Integrated Boost Flyback Converters (IBFC) was described in the study [27]. The boost sub-converters offer varying loads while charging the battery bank by interlacing with the flyback sub-converters. The recommended converter is modelled in MATLAB/Simulink to verify analytical findings utilizing solar panel input power. We describe an insulated circuit architecture appropriate for heavy-step-up processes over a wide voltage supply range in this inquiry as a response to [28].

An all-purpose Active Clamp Flyback converter (ACF) manages the excess power after a current-fed resonant PP converter functions as a DC transformer (dcX). Empirical findings support the research by proving the converter of choice is suitable for MHz high step-up dc-dc conversions. With its configuration consisting of an Interleaved Flyback Microinverter (IFMI), the novel microinverter architecture introduced in an article [29] is known as IFMI. Two-phase interleaved flyback converter is used for the DC-DC power conversion in the micro inverter's two-stage design.

In contrast, the H5 inverter architecture is used for the AC conversion step. The suggested converter's power conversion and reference tracking stability have been verified via simulation and experiment. Furthermore, the benefits and drawbacks of the proposed device architecture have been analyzed in-depth, and the potential for further development has been explored [30].

The two-stage micro inverter uses a two-phase interleaved flyback converter for the DC-DC power conversion. In contrast, the AC conversion stage uses the H5 inverter architecture. Simulation and experiment have been used to confirm the recommended converter's power conversion and reference tracking stability. The possibility for further development has also been examined, as well as the advantages and disadvantages of the suggested device architecture [31].

According to the research [32], a Zeta Power Factor Correction (PFC) converter improved power quality when charging the batteries of electric vehicles by lowering the switch voltage stress on PFC devices. Charger efficiency over Zeta PFC converters is increased, and PFC stage losses are decreased when the switch voltage concerning the supply voltage is less stressed. By utilizing fewer sensors and fewer magnets, cost and size can be decreased. Comparisons reveal reduced device stress, enhanced PQ, and elevated effectiveness [33].

There are now fewer power-switching components in the circuit because of the Cascaded H-Bridge Multilevel Inverter (CHBMLI) development. The PWM output voltage can be produced using a multicarrier pulse width modulation approach. Constructing a field programmable gate array facilitates the realization of the method and the verification of the simulation results over a wide range of modulation indices. The findings offer a fresh prescription for an MLI architecture suitable for real-world use cases [34].

Creating a revolutionary hybrid Multilevel DC-Link Inverter (MLDCLI) to handle more levels with fewer switches led to improved sinusoidal output voltage synthesis. The design contains an unidentified module and a unique H-bridge. The proposed dual-bridge MLDCLI employs a Phase Derivation (PD) Multicarrier Pulse Width Modulation (MC-PWM) technique after being examined in an FPGA environment. The output voltage as a function of frequency can be used to calculate the Total Harmonic Distortion (THD), and a harmonic spectrum can be used to demonstrate the removal of non-fundamental frequency components. This makes voltage regulation suitable for new applications [35].

In order to optimize the advantages Of Distributed Generation (NHOA-DG) in a deregulated electrical system, investigators devised a new hybrid optimization technique. This mathematical model has examined the steady-state operations of the distribution network. A different search technique compares the optimization results with their solution, such as a Genetic Algorithm (GA) or a Micro Genetic Algorithm (MGA).

The investigators at developed a new hybrid optimization technique to maximize the benefits of Distributed Generation (NHOA-DG) in a deregulated electrical system. This simulation was done to examine distribution network steady-state operations. Another search method, such as a Genetic

Algorithm (GA) or a Micro Genetic Algorithm (MGA), contrasts the optimization results with their solution and presents a Renewable Energy System (RES) with a multilevel inverter to provide a lossless power supply to the load. The system continuously checks the batteries' charge state and compares it to a preset threshold for current power consumption.

The approach to testing employed in this study is ineffective for identifying the split-relevant capacitor size. The design method also disregarded load state, leakage inductance, and segregated MPPT conversion efficiency. This study suggests a flyback DC-DC converter design to decrease primary power switch voltage spikes and boost power conversion efficiency, examining the split resonant capacitor, leakage inductance, and load variations with the innovative converters to analyze the operation of the DC-DC flyback converter. The flyback converter MPPT is needed for the power switch voltage spike, and power conversion efficiency is developed using theoretical investigations.

3. Proposed Method

In Figure 1, the equivalent circuit is a PV cell model. This configuration is modelled as a single diode. The depletion area is based on the premise that reassembly loss will be minimal. The one-diode form is often used in PV applications due to its relative ease of use. For accurate modelling and simulation of PV cells, parallel and series resistance is required.

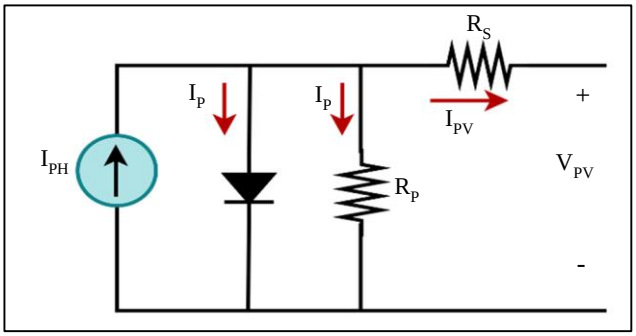

Fig. 1 PV equivalent circuit model

$$I_{pv} = I_{PH} - I_D - I_p \quad (1)$$

$$I_D = I_o e\left(V_D / \alpha V_{T-1}\right) \quad (2)$$

$$V_T = kT / q \quad (3)$$

$$V_{pv} = \alpha V_T 1n \frac{\left[I_{PH} - I_{pv}\right]}{I_o} + 1 \quad (4)$$

Where is the humidity electrical power, solar power electricity, diode integrity, opposite saturated state of the diode, PV cell production of electricity, containing high electricity, shorter circuitry cell electricity, transistor electricity, Boltzmann's pervasive, and electrode-like expense in equations (1), (2), (3), and (4)? The resistance in the parallel direction is represented by, the series resistance is denoted by, and the PV cell humidity is characterized by equation 2 and Figure 1 can be used to compute the current generated by a PV panel in equation (5),

$$I_{pv} = I_{PH} - I_o\left[\exp\left(\frac{q\left(V_{pv} + R_S I_{pv}\right)}{\alpha kT}\right) - 1\right] - \frac{V_{pv} + R_S I_{pv}}{R_p} \quad (5)$$

R_s = 0 and R_p = infinity in an ideal condition. Although this perfect state is unattainable, manufacturers might strive to enhance their items by lessening the effects of both kinds of resistance.

Flyback converters' primary function is to change the direction of electrical current flow from AC to DC while maintaining galvanic isolation between the two ends of the circuit. A flyback converter stores energy when power is applied and releases it when the circuit's current is cut off. A flyback converter imitates the behavior of an isolated switching converter when used in conjunction with a step-down or step-up changer. Flyback converters are capable of controlling several output voltages with different input voltages. The design of flyback converters is more straightforward and less involved than those of other switching power supply circuits. The word "Flyback" is an example of how the on/off switch is incorporated into the design of Flyback converters. Figure 2 depicts the flyback converter's basic circuit diagram of power flow.

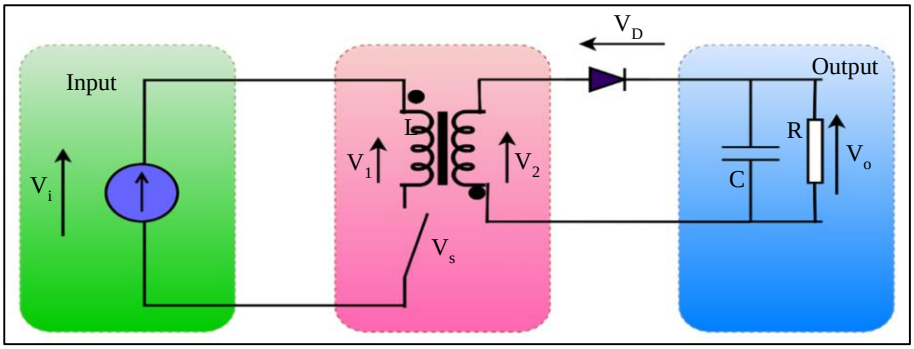

Fig. 2 Circuit of a flyback converter

An electrical current's polarity can changed using a flyback converter. Flyback converters change the flow of electricity from AC to DC and vice versa, similar to how switch-mode power supplies operate. The flyback converter operates on a non-linear switching supply as its foundation. The fundamental concept underpinning the design of flyback converters is using a flyback transformer, which stores magnetic energy and functions as an inductor. The Flyback converter architecture uses a control mechanism to drive the switch and regulate the signal. The transformer is magnetized or demagnetized using the ON/OFF switch. The switch in a flyback converter could be a FET, MOSFET, or a straightforward transistor.

In a flyback converter, a rectifier transforms the voltage of the secondary winding into a pulsating DC output. The transformer's winding could also lose power if the rectifier does so. The rectifier provides DC voltage, which the capacitor amplifies and smoothes for various applications the Flyback transformer stores magnetic energy in a flyback circuit by acting as an inductor.

A flyback transformer's primary and secondary windings have two connected inductors. The operating frequency of a standard flyback transformer is close to 50 KHz. The SMPS mode is necessary for flyback converters to function. Even when the switch is turned "ON," the load is not receiving electricity. The drain voltage is zero because the primary winding is fully charged.

The power is stored in the magnetic inductance of the transformer, the current rises linearly, and the diode works in its reverse-biased state. The output is coupled to the secondary winding of a capacitor, which stores the energy. When the switch is OFF, energy still travels from the input to the load despite the magnetic field's action and the polarity reverse. When this occurs, voltage balancing also begins. In this case, the core would deliver energy to the load to correct it. The process is repeated until the power runs out or the switch is returned to the "ON" position.

A wide range of DC-DC conversion techniques are frequently used in PV systems. Buck-boost converters are comparable to flyback converters. It is possible to achieve voltage isolation at the place of origin by only switching the polarity of the transformer and slicing the inductor. The flyback converter receives its unregulated DC input voltage from the PV panel.

To keep the reference output voltage constant, the gate drive circuit connects the primary side of the isolated inductor to the MOSFET switch. A rectifier diode and resistor adjust and regulate the power from the transformers' secondary circuit. An inside diagram of a flyback converter. The flyback converter's output voltage can be calculated using the following expression: 6.

$$V_o = \frac{N_2}{N_1}.\left(\frac{D}{1-D}\right).V_i \qquad (6)$$

Equation 6 shows the input flyback voltage V_i, the duty cycle D, and the converter's turn ratio $\frac{N_2}{N_1}$. The schematic for a flyback converter (Figure 3) shows the following power flow. The capacitor also reduces the solar current's harmonic content and smoothed it out. When the MOSFET switches are switched on, the flyback converter's primary winding and magnetizing inductance receive current from the solar array. Current cannot flow through the diode while the switch is turned on because it is biased in the opposite direction. The magnetic field energy of the magnetizing inductance is released into the grid as current when the switches are deactivated. The flyback converter defines the configuration as a wattage-controlled current source.

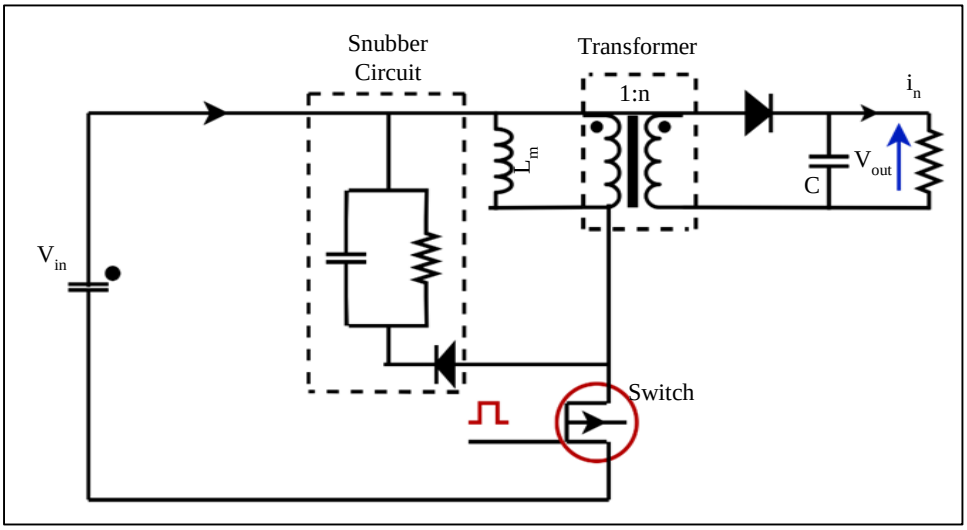

Fig. 3 Power flow of flyback converter

The objective of solar power plants is to generate as much electricity as is practical. The PV plant's layout and construction impact how much energy is generated in addition to solar radiation. Consolidated integrator designs, one converter per cord, one adapter per PV board, and stand-alone Maximum Power Point Tracking (MPPT) architectures are just a few of the numerous ways converters can be incorporated into PV plants.

To maximize the internal voltage characteristics of the solar cells and keep them operating as effectively as possible, many modern converters integrate MPPT monitoring. Unmatched PV panels are a frequent reason for solar power system failure. For optimal power conversion efficiency, every PV panel in a solar power plant needs to be installed with a Flyback DC-DC converter.

A capacitor, a transformer, a diode, and a capacitor at the output make up the core of a flyback converter. The DC voltage generated by the PV panel is stored in the input capacitor. A semiconductor switch opens and closes when the converter is turned on, allowing current to pass into the transformer. Since the transformer alters the input voltage to produce the desired output voltage, it is crucial for transforming energy. The diode ensures that current only flows in one direction, preventing any feedback from the PV panel. At the very least, the output capacitor levels off the DC voltage. Due to its small size and versatility, the Flyback DC-DC converter is a crucial component of any photovoltaic solar system, enabling efficient energy transmission and voltage control. Figure 4 illustrates the flyback DC-DC converter's structure for each solar power plant PV panel.

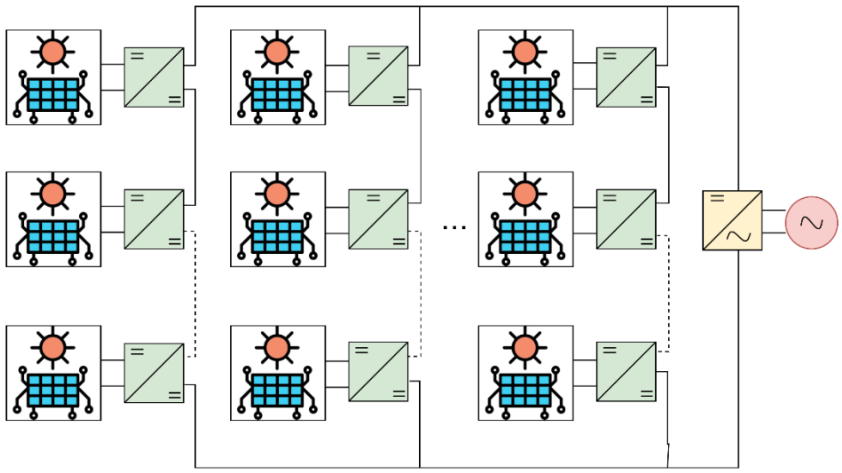

Fig. 4 Structure of flyback DC-DC converter per PV panel in a solar plant

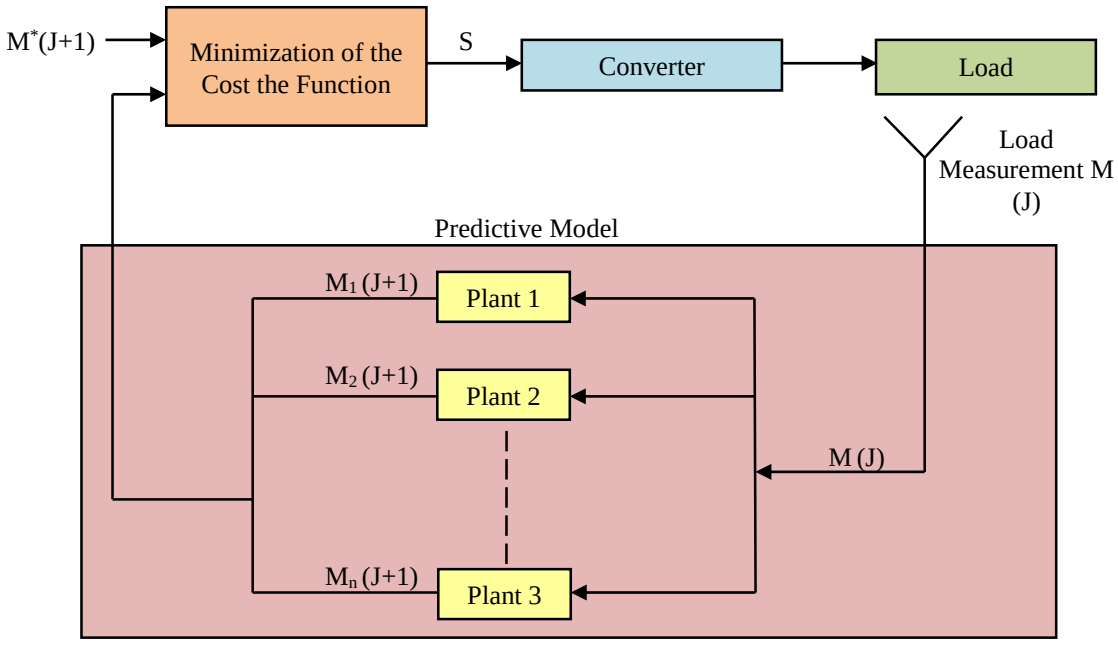

Fig. 5 MPC scheme for electrical power inverters

The output of the affected panels and the electrically connected boards can be decreased by mismatching, depending on the PV plant's architecture. Our study aims to separate PV panels; thus, we concentrate on the maximum power point tracking method depicted in Figure 4. WITH THIS ARRANGEMENT, each PV panel may produce the total amount of power under every solar plant situation. The leading power point tracking system converters must also satisfy several other criteria, including cheap cost and high efficiency.

Several writers have proposed employing series-connected converters to boost converter efficiency. The concept behind this type of converter is that it only controls a small portion of the energy that is transferred to the grid. As a result, the outcomes are highly productive. This arrangement is perfect for applications requiring a greater final voltage than the supply voltage. The Type Connected Flyback converters' static properties are described in depth. Theoretical analyses support the valuable information from a 300W SCF converter and prototype simulation.

Model Predictive Control (MPC) techniques were initially utilized in power electronics, namely in power-hungry machines with slow switching rates, and switching frequencies couldn't rise due to the lengthy computation time needed by the control approach. In contrast, curiosity about using MPC in electrical circuits has significantly increased over the last decade due to quick and effective processing units.

The distinguishing feature of MPC is its ability to anticipate target parameters up to a given time horizon. The optimal switching state can be discovered by minimizing an expenditure function with the variables expected. For making predictions, use a state space model, a discrete-time model. The MPC for power electronics converters can be developed using the procedures that are listed below.

Input and output voltages and currents are represented, along with the switching states of the power converter.

- First, the anticipated system performance has been described by defining a cost function.
- Acquiring discrete-time models that allow looking into the future and predicting exactly the variables under authority are likely to react.

The following responsibilities should be taken into account when designing a controller:

- Anticipate how the controlled variables will act in all potential transition stages.
- Each prediction's cost function should be analyzed.
- Choose the transition state that results in the lowest cost.

Figure 5 depicts the overarching structure of converting power electronics using MPC. The model uses the observed variables to predict the controlled variables for each change in condition, electricity, power, and actuation $\widetilde{M}(J+1)$. The standard structure of the cost variable g under the reduction constraints looks like the following:

$$g = \left[\tilde{M}_1(J+1) - M_1^*(J+1)\right] + \lambda_1\left[M_2(J+1) - M_2^*(J+1)\right] + \ldots + \lambda_n\left[\tilde{M}_n(J+1) - M_n^*(J+1)\right] \quad (7)$$

Where λ is the relative importance of each goal, each potential switching state is analyzed for its effect on the cost function g, and the one with the lowest value is saved for later use. For example, in Figure 5, the power converter of any configuration and phase count may be used. A powered item, the power grid, or an active or passive load can all stand in for the generic load, as depicted in Figure 6.

Maximum Power Point Tracking at the highest level of capability is necessary to harvest the total amount of electricity from solar panels due to the PV systems' low conversion efficiency, a key hurdle to their widespread adoption.

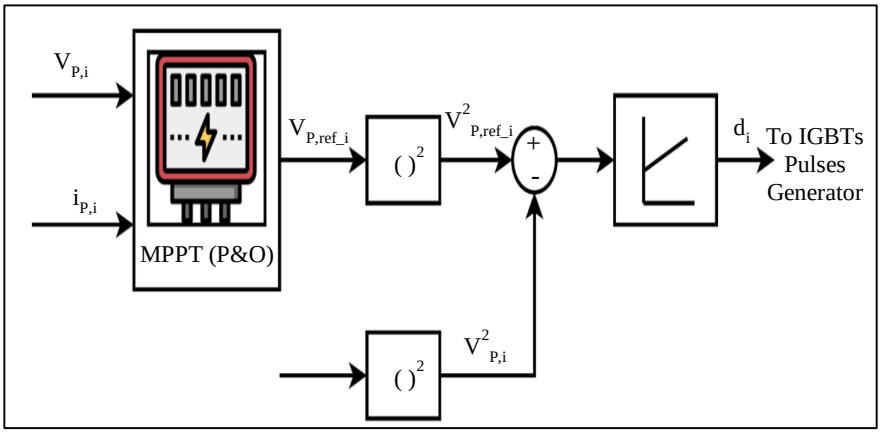

Fig. 6 Model of MPPT algorithm

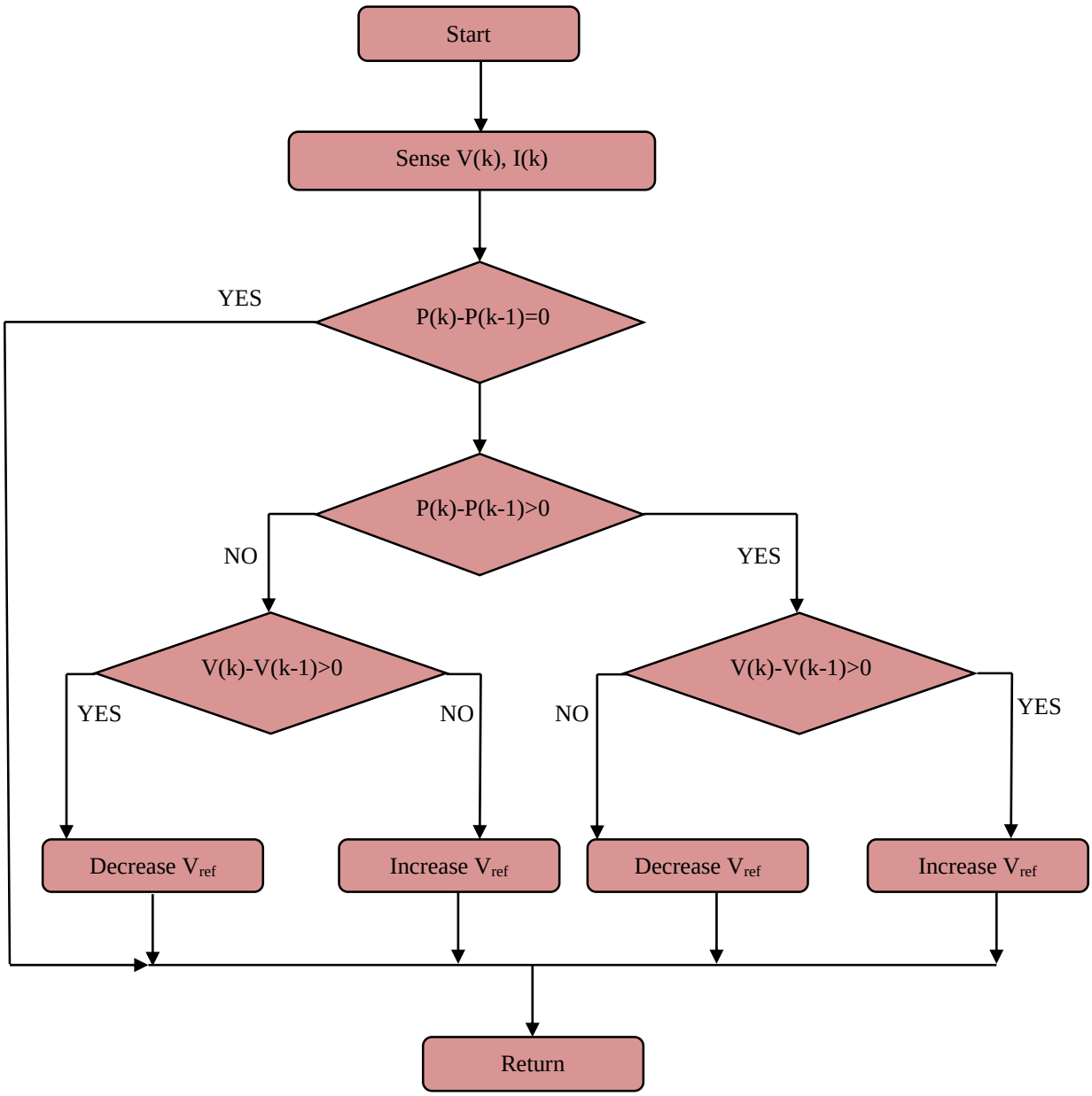

Fig. 7 P&O algorithm flowchart for PV systems

Low insolation is necessary for operation. By absorbing as much solar energy as possible during low insolation periods, a considerable potential to improve system performance is presented. As a result, an MPPT controller and converter can significantly minimize the amount of PV required. An MPPT controller connects the solar module to the resistive load, ensuring maximum efficiency.

A power electronic converter (DC/DC converter) has a distinctive control algorithm, this controller. The MPPT method thus extracts the total amount of energy from the PV panel. The MPPT employs isolated flyback DC-DC converters. From the viewpoint of the PV module, altering the duty ratio causes the intake impedance of the flyback converter to change, resulting in increased efficiency. The MPPT controller begins at this point where maximum current and voltage intersect.

Several MPPT strategies can be used, most of which can be categorized as direct or indirect. The natural techniques are based on the slope of the P-V characteristics or other connections based on this principle. The maximum power point is occasionally reached despite the P&O method's widespread use and respectable performance. Additionally, P&O is slow and struggles to adapt to the changing sun well.

A model predictive control strategy for enhancing the P&O method's performance by foreseeing faults one timestep

in the future is the critical contribution of this section. The P&O algorithm has proven itself as the standard MPPT choice for commercial and industrial PV systems because of its simplicity and high efficiency. Regrettably, the P&O algorithm results in oscillations that reduce the effectiveness of the power system. The P&O behaviour used to build the control mechanism for the energy system seen in Figure 7 is reviewed in detail.

A flyback converter is utilized as the DC/D C converter. The MPC uses the default voltage provided by P&O to calculate the future flipping situation. The ideal switching state can be chosen by maximizing the cost function g in Figure 5, which considers the likelihood of making an error in the following sampling period. The anticipatory microcontroller receives a PV system's voltage, electrical current, and average power. Due to its low cost and simplicity of usage, the P&O approach has become the most popular MPPT methodology. Following initial voltage, current, and power P& readings from the PV panel, the operational voltage of the PV module is changed, yielding a new power P the distinction between the before and after the change. The operating voltage perturbation brings the operating point closer to the maximum power point if the deviation is positive.

Currently, the voltage is constant V_{mpp}, and the PowerPoint P_{mpp} is at its highest. Therefore, modifying the direction of the additional perturbation added to obtain the MPP is unnecessary. If the outcome is unacceptable, the algorithm will shift in the opposite direction. The impact of a disturbance on power should be similar to that on voltage in terms of approach. If the two values travel in opposite directions, the voltage standard must be turned around. Continue doing this until the PV panel has been fully utilized for energy.

Smaller perturbation steps can reduce the algorithm tremor. As a result, using short increments reduces the MPP tracker's response time; this problem is avoided by employing a perturbation process with variable step sizes. This approach has the advantage of being famous and straightforward to utilize. Figure 7 depicts this pattern, assuming the operation is initiated at a PV voltage below the MPP. The P&O algorithm maximizes PV power by increasing PV voltage when PV voltage is less than V_mpp and minimizes PV power by decreasing PV voltage (red arrows) when the MPP is to be reached. Lastly, the P&O protects the MPP and the PV system's three-point behaviour, guaranteeing maximum output.

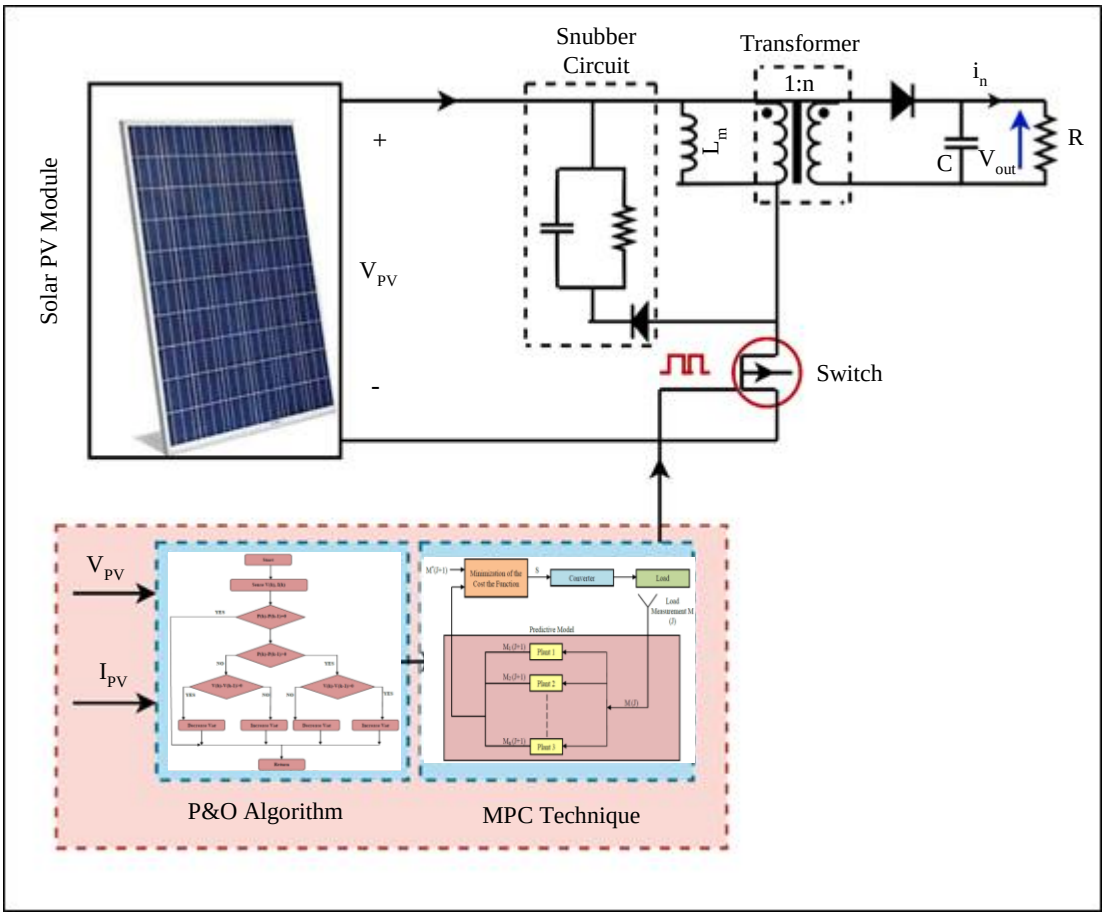

Fig. 8 Proposed scheme of the MPPT system

However, it has some drawbacks, including difficulty monitoring power under various air conditions and power loss caused by this disruption. A flowchart outlining the P&O MPPT approach is shown in Figure 7. Changes in the current and voltage generated by a photovoltaic source are a function of the ambient temperature and sun irradiation over time. The Maximum Power Point (MPP) is the unique operating condition when the current and voltage are at their most excellent levels, and the most energy may be harvested. Although many other algorithms are available, the P&O method is utilized for MPPT. Monitoring the voltage and current of PV panels allows their power to be determined. The duty ratio could be lowered by improving the voltage and capacity. Maintaining a positive energy and a negative voltage change is necessary for increasing the duty ratio.

Maximum Power Point Tracking (MPPT) can be used to determine the duty ratio and flyback converter firing pulses the P&O algorithm experiments with positively and negatively changing the PV voltage to maximize energy production. By employing powerful algorithms to track the MPP and squeeze every last bit of power out of a PV array, this work improves upon the MPPT technique. Figure 8 shows the PV system's high-level block schematic, showing how the flyback converter and MPPT technology fit into the bigger picture. The PV system comprises a solar PV module, flyback converter, MPPT, and a resistance load.

A voltage converter is employed to determine the PV electricity; meanwhile, a standard DC detector is used to determine the PV voltage (type 1NA169). For the flyback converter's primary MOSFET to drive the opt-coupler IC (PC 817), the microcontroller must send a Pulse-Width-Modulated (PWM) signal from one of its pins. To maximize power transfer from the PV module to the load at all temperatures and irradiance levels, the MPPT approach analyzes data from the two sensors. It modifies the duty ratio of the flyback converter.

Connecting the photovoltaic panel to the load resistor is where the DC-DC converter comes into play: the MPPT method and the flyback converter work to determine the PV module's peak power output. The MPP is kept constant using the MPPT technique, which supplies the proper duty cycle to the flyback converter regardless of the sun irradiation or temperature. The PV system is globally stable despite regional variations in output voltage and irradiance, as shown by a duty cycle form. The model also provides the flyback converter's maximum switching frequency (95 kHz), which is proved to be consistently lower than it.

Finally, the provided simulated circuits test the dependability of the MPC under realistic circumstances, ensuring that the P&O algorithm can maintain the PV panel's peak efficiency (reference variations) despite varying irradiance levels (line variations) and fluctuations in voltage at the output port (load various), which typically occur due to the converter's conjunction within the microinverter.

The following assumptions are used to investigate the converter and its multiple modes. The converter operates in DCM and steady-state current ($N_1(1,n):N_2=1$ the n-th initial windings) thanks to the single-core ferrite-linked inductors (flyback transformers) with these characteristics. Resistances are ignored, and the resonance leakage is defined as L_{lk}. There is a duty cycle on the main switches () and a duty cycle D_2 on the secondary switches.

In this article, we describe the magnetizing inductance L_m, the commutation time t_f, and the switching frequency f. For this architecture to work, the photovoltaic panels attached to the inverter needed to have as much energy extracted from them as possible in a single switching t_r cycle.

The flyback converter's magnetized core might be shorter if only one PV panel was used to supply power rather than the longer length required for many panels. Since the switching time was broken up into chunks based on the number of primary windings, t_r it is divided into three pieces in this analysis. The snubber network harnesses the flyback transformer's leakage inductance, which also reduces the dv/dt of the main switches.

The current from the leakage inductance charges the snubber capacitor, which is subsequently discharged into the input section V via the opposite diode in the main switch. The efficiency of the topology was improved by following these steps. There are six distinct phases to the operation of each PV panel. Some of the presumptions made during the development of the suggested converter are as follows:

- The circuit is in a steady state of operation.
- When compared to the magnetizing inductance, the leakage inductance is negligible.
- No loss occurs in any of the energy storage components.

The suggested converter's duty cycle may be calculated using the following equation (8), which is valid under the conditions above:

$$D = \frac{2nV_o}{V_s + 2nV_o} \tag{8}$$

Isolated-type converters are very picky about their transformer designs. Each converter's turn ratio must be precisely determined using the following equation (9).

$$n = \frac{N_1}{N_2} \le \frac{V_s x \bar{D}}{V_o\left(1-\bar{D}\right)} \tag{9}$$

Where $\bar{D}$ is the highest duty cycle value, and V_S does the proposed converter require the lowest DC input voltage.

The main intermittent Flyback converter may be set up in several ways, like any other DC-DC Flyback type converter. Therefore, the suggested topology necessitates the design of the snubber circuit components. Careful construction of snubber capacitors is required to establish a ZVS state at the turn-off. They need to reduce the switch's voltage till their current is zero. As a result, it can determine C_{S1} and C_{S2} using the following equation (10),

$$C_{S1} = C_{S2} > \frac{\bar{I}_{SW}\, t_f}{2V_S} \tag{10}$$

Where t_f is the timing of switch failure and $\bar{I}_{SW}$ is the maximum power through the switch at switching off. For example, the following equation (11) may get this value.

$$\bar{I}_{SW} = \frac{\bar{P}_o}{\eta V_S \bar{D}} \tag{11}$$

Where $\bar{P}_o$ is the peak power from the converter, and η is the efficiency. For the above calculation, η it is often used as the worst scenario, about 80%.

By controlling the rate of current increase upon turn-on, leakage inductors may guarantee a ZCS situation. Finally, the following equation can be used to determine L_{lk1} the next L_{lk2};

$$L_{lk1} = L_{lk2} > \frac{\bar{V}_S + 2nV_o}{2\Delta I} t_r \;\&\; \Delta I = \frac{P_o}{\bar{V}_S D} \tag{12}$$

Where t_r is switching on time increase, $\bar{V}_S$ is the maximum value for DC input, P_o is the minimum attainable electrical voltage, D is the lowest possible duty cycle, and ΔI is the fluctuation of the leakage inductance current.

Finally, the following equations may be used to determine the values of the snubber inductors L_{S1} L_{S2} and the magnetizing inductors L_{m1} L_{m2} in equations (13) and (14).

$$L_{S1} = L_{S2} \geq \frac{2C_S V_S^2}{(1-D)^2 i_S^2} \tag{13}$$

$$L_{m1} = L_{m2} \geq \frac{2V_S^2 D^2}{f_S \bar{P}_o} \tag{14}$$

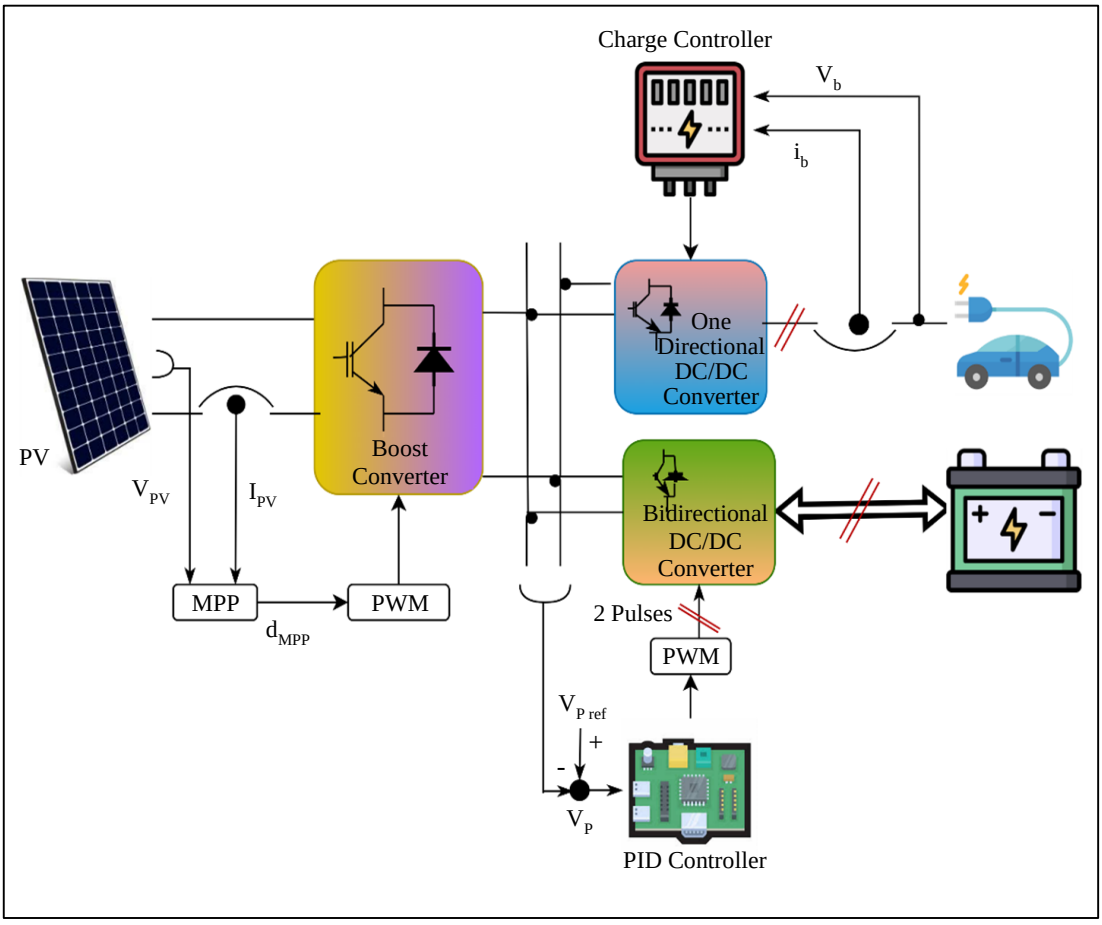

Fig. 9 EV's energy management using PV systems

On the other hand, the electrolytic sulfur converter may function in either way as a step-down transformer. It controls the charging and discharging cycles of the ESS. It also helps maintain a consistent voltage on the DC bus. The MPPT converter and EV charge converter are the planned system charging converters. There is a DC/DC converter in both. The electric vehicle charging converter, however, is a step-down design. The MPPT converter, on the other hand, is a bidirectional one. It may function in both directions. As can be seen in Figure 9, the two converters may use the same topology. However, the topology's functioning may be tweaked to serve as a one- or two-quadrant converter.

Continuous conduction mode operation of the converters is expected. To keep your EV charged safely and securely, utilize the EV controller. The MPPT conversion regulator additionally regulates the charges and discharges of the MPPT. This also controls the DC link frequency. Maximum Power Point Tracking is the last and final microcontroller, which aids in drawing the most possible energy from the PV system. Information on these controllers is provided below. The maximum power point tracking controller may significantly boost system usage. In practice, the MPPT may be used in various ways. The "Perturb and Observe" methodology is utilized in this study. The steps involved in this application are as follows:

- The boost converter is set to an advised starting duty ratio.
- After that, the PV's current and voltage are measured.
- Variation in PV power is estimated.
- To achieve an MPPT condition, the controller must output a specific duty ratio for the boost converter.

The EV charger controller regulates the associated converter to manage the EV charging process. Two nested loops are often used for control. The outermost loop represents voltage, while the innermost represents current. This method employs a steady current and voltage throughout. A PID controller is used in this application.

Distribution, State of Charge (SoC), battery life, duration of appointment, and other variables contribute to how HEVs behave when plugged in. There might be less uncertainty when calculating the effects of EVs if all these factors are adequately characterized. This article uses the SVM method to forecast the overall charging requirements of EVs. Electric Vehicles (EVs) may technically be powered by either gasoline or electrical. Since EVs run in part on energy and in part on fossil fuels, the cylinder symbolizes the fuel merchant. Researchers still need to figure out how to make sense of the distribution of fees in such cars.

Two methods, exact and structured charging, are proposed to accomplish this. Electric vehicles can only charge during certain hours if they use integrated charging. Customers' typical routines throughout the day informed these times. This implies drivers may begin recharging their vehicles after work during less busy off-peak hours (about 6 PM).

$$d(f_{start}) = \frac{1}{\gamma_1 - \gamma_2} \gamma_1 \le f_{start} \le \gamma_2; \gamma_1 = 19, \gamma_1 = 20 \quad (15)$$

In equation (15), Smart charging, $d(f_{start})$ which allows cars to charge following the electrical load curve of the microgrid $\gamma_1 - \gamma_2$ and tendering offers by the power suppliers, is the second charging pattern that may be considered. The standard deviation function is used to represent this tactic, as seen below in equation (16),

$$d(f_{start}) = \frac{1}{\sigma\sqrt{2\pi}} r\left(-\frac{1}{2}\left(\frac{f_{start-\mu}}{\sigma} \right)^2 \right) \mu = 1.5, \sigma = 3.2 \quad (16)$$

When the EV's start time μ is known, the battery's System on a Chip (SoC) $\sigma\sqrt{2\pi}$ can calculate how much power it will need. Calculating the SoC requires knowledge of the typical distance travelled by each vehicle. The standard length of each electric car may be computed using the following equation (17).

$$d(s) = \frac{1}{s\sigma\sqrt{2\pi}} r \frac{-(In(s)-\mu)^2}{2\sigma^2} S > 0 \quad (17)$$

Using $s$one can easily calculate the battery SoC using the equation (16) below,

$$SoC = \begin{cases} \frac{ED - s}{ED} x100\% & s > ED \\ s \le ED \end{cases} \quad (18)$$

Where ED is the total electricity range (the point beyond which the car would not operate). Literature suggests that $ED - s$ it may range from (22), (25), (28), and (33), depending on the vehicle in question. Ideally, know the System-on-Chip (SoC) and battery capacity, then use the following equation (19) to predict the charging time,

$$f_s = \frac{E_{bat} x(1 - SoC) xSOS}{\eta_e xL} \quad (19)$$

As can be seen from Equation (19), the charging period f_s is also affected by the charger's kind (L_e) and effectiveness (s).

The computation process uses the information gathered by light-sensitive sensors as crucial inputs. Before sending data to the microcontroller, the analog inputs from the sensors

are converted via an Analog-to-Digital Converter (ADC). The Arduino microcontroller determines the servo motors' steep angle and movement based on the transmitted digital signals. The microcontroller stays in its present state if the light density on both sensors is equal; otherwise, it drives motor activity until signals from both sensors are not equal. When the angle of incidence of light on the detectors is uniform, the position of the PV panels is locked to achieve maximum output.

Proper battery storage or grid connection synchronizes and collects the resulting voltage diversity. When the tracker detects the highest intensity of light falling perpendicular to it, it moves to that spot until the light angle changes again. The approach is built with an eye toward both current and historical tracking. It is calculated accurately based on installation location and intended use of the generated power.

This device incorporates features from both open-loop and closed-loop control algorithms to counteract the unpredictability of installation, assembly, and encoder mounting and maintain a reasonable price point. The suggested approach guarantees the least expensive capability costs and the most efficient generation possible.

4. Analysis and Discussions

Maximum power point tracking efficiently delivers the electricity produced by solar cells to the power grid by utilizing a flyback transformer. Optimizing the DC voltage and current at the interface is required to maximize energy harvesting from a solar array. The second objective of the control technique is to regulate the MPPT and direct current from the PV source.

It is changed into alternating current using a grid interface expanding converter. Grid alternating current is synced with grid frequency using control methods to reduce harmonic interference and produce a unity power factor. A dispersion capacitance, which functions as a buffer and power regulator, is positioned between the PV input and the flyback DC-DC converter.

One of the most efficient options for supplying the increasing need for electricity in households, businesses, and industries is solar power, which is increasingly gaining popularity. The conversion of sunlight into power using solar photovoltaic systems has recently piqued the interest of many academics and business leaders. The fundamental challenge of solar energy production for the effective daily/hourly oversight of electrical power generation, delivery, and storage spaces is that electricity generation from photovoltaic systems is intermittent owing to weather.

Therefore, it is essential to make accurate short-term estimates of the power output of PV systems for various reasons, such as facilitating the choice of the energy sector, participating early in electricity auction systems, and making the best use of available resources.

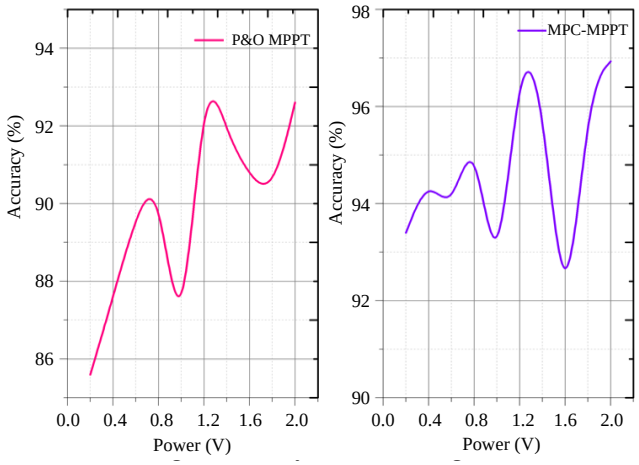

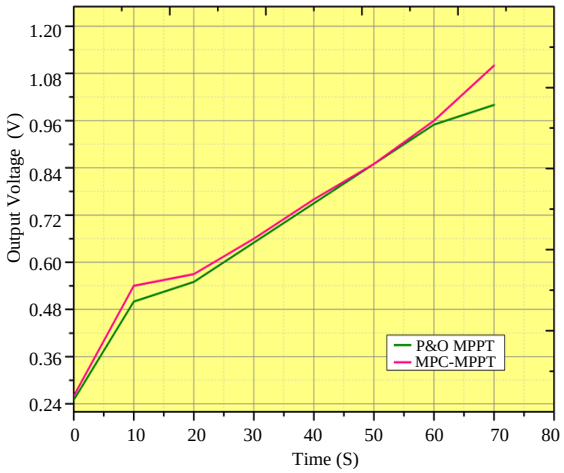

Fig. 12 MPPT performance varies with output voltage

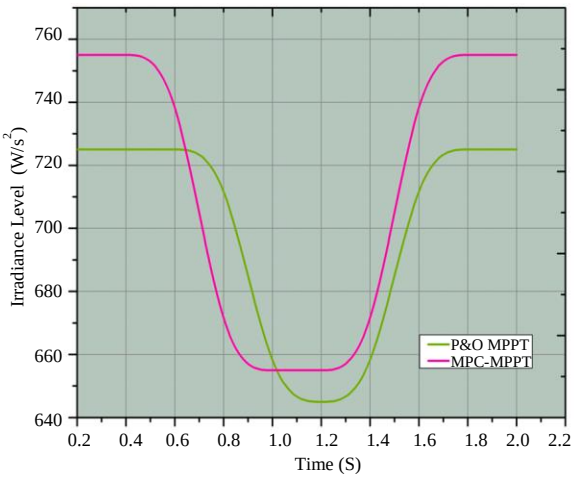

Fig. 12 MPPT performance varies with light intensity

The proposed approach successfully and correctly monitored the maximum power despite the constantly shifting weather circumstances, as shown in Figure 10. The recommended MPC methodology outperforms the P&O MPPT method to follow the MPP at 0.01 and 0.015 step sizes. Additionally, the oscillations near MPP for both step sizes are lower than those brought on by the P&O MPPT technique.

Regarding tracking accuracy in variable weather conditions, the suggested method exceeds the P&O MPPT, averaging an accuracy of about 95.34% for both step sizes. Tracking accuracy for the MPC-MPPT is 96.93% with 0.01-step size and 96.89% with 0.015-step size.

The MPPT standards must be met for the PV system to function correctly when exposed to irradiation exceeding levels. Tests were conducted at various irradiance levels to validate the MPC and P&O algorithms. The simulation shown in Figures 11 and 12 indicates that the PV system produces 1000 W/m2 for the first 13 ms before dropping abruptly to 600 W/m2. The second phase of a PV microinverter's operation is taken into consideration in the simulation. PV power is consistently at the MPP voltage for both irradiance scenarios in the simulation, demonstrating the efficiency of the P&O algorithm and MPC, except for a lengthy time between 13 and 18 milliseconds, during which the P&O takes five milliseconds to follow the new MPP condition.

Once the new MPP condition has been reached, and assuming the PV system is operating normally, the PV voltage will accurately mirror the stable three-point behaviour of the P&O. Experimental assessments of the converter's input and output voltages and currents were made (Figure 11), and the converter's performance was evaluated using this information. The power from all the PV panels was combined to determine the overall electrical input power employed in this calculation.

On the other hand, the power output was measured using the load. The formula = 100 / was then used to calculate the converter's efficiency. Data on the converter's efficiency were gathered at various solar radiation levels and times. Figure 13 is an illustration of the results. During the middle of the day, when the PV panels produced electricity close to their rated value, the best efficiency (96.7%) was measured. Table 1 illustrates the P&O and MPC comparisons.

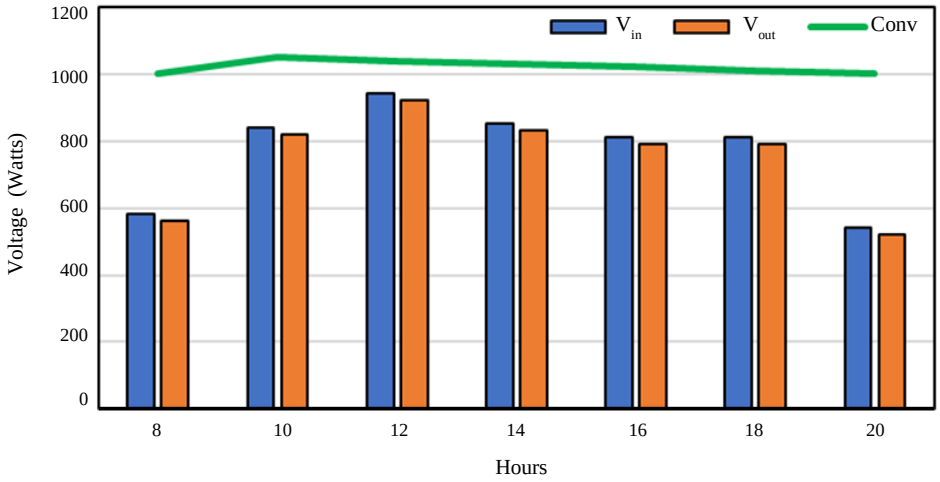

Fig. 13 Performance analysis of flyback converter

Table 1. P&O and MPC comparisons

Time (Hrs)	P&O MPPT (%)	MPC-MPPT (%)
10	62.5	81.5
20	69.2	85.4
30	71.9	81.8
40	70.2	86.3
50	64.7	89.6
60	62.4	71.4
70	70.7	76.3
80	73.1	86.9
90	70.5	84.4
100	85.9	98.8

The converter's dependability and efficiency are susceptible if the system temperature rises without first conducting a thermal analysis. This research is crucial for identifying areas that could be improved or rewritten. Thermal analysis is critical in determining a flyback converter's efficiency for solar photovoltaic systems. The rise in converter temperature and its effects on the effectiveness and dependability of the system have been examined. The total efficacy and trustworthiness of the flyback converter for solar photovoltaic applications strongly depend on the findings of the thermal analysis. Analysis must be done before and throughout the system's development to ensure optimal performance.

In general, the information provided in the previous table on the thermal behaviour of the flyback converter under different MPPT algorithms helps determine which MPPT approach is optimal for a specific solar PV application. Figure 13 illustrates the performance analysis of the flyback converter.

In addition to a statistical performance analysis, this work thoroughly analyses different converters. More mechanical separation from the FC's result (low voltage) and the DC connector (high voltage) is required when the voltage differential between them is more significant. In improved flyback generators, rectifying diodes are subjected to high voltage and experience considerable stress. However, the operation is interrupted (to prevent core saturation), the neutral potential is substantial, and the core is underused despite the current flowing through the single circuit.

Since a current-fed entire circuits converter is a hard-switched converter, operating at 10kHz necessitates larger magnets and filters, increasing the converter's size. Because of the need for the current clamping mode, these circuits are essential for lowering switch load. Further switches are needed to complete the active brake (or reset) circuit, and the associated triangular current waveforms increase conduction losses (Figure 14). The DC-DC conversion from 40 V to 380 V operates at a maximum efficiency of 96.7%.

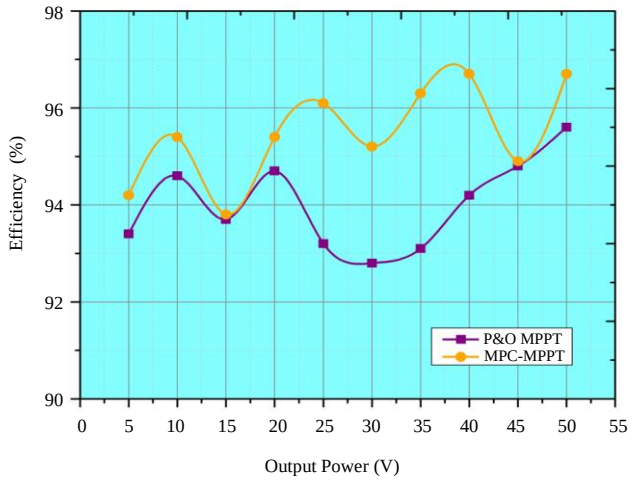

Fig. 14 Measured efficiency vs Power

The proposed MPC-MPPT technique is tested under various pressures to show its effectiveness and resilience. In the case shown in Figure 15, the load changes, but the temperature and solar radiation stay constant at 1000W/m2 and 298°F, respectively. The image shows that the load is maintained at 35.5 until the timer hits 0.03 seconds, which reduces to 18.5. The load is again altered after 0.06 seconds, this time to 35.5. Figure 16 displays the P&O method and the suggested MPC-based MPPT's maximum power tracking. The graph below shows how well the proposed strategy sustains peak power under various loads. The MPC-based MPPT strategy outperforms the P&O strategy when coping with varying loads.

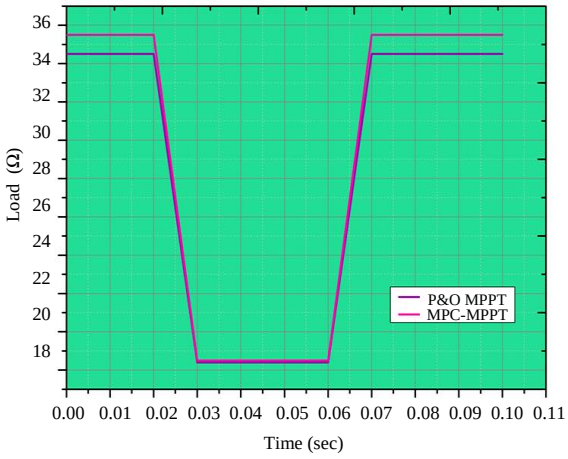

Fig. 15 Variation in the load case

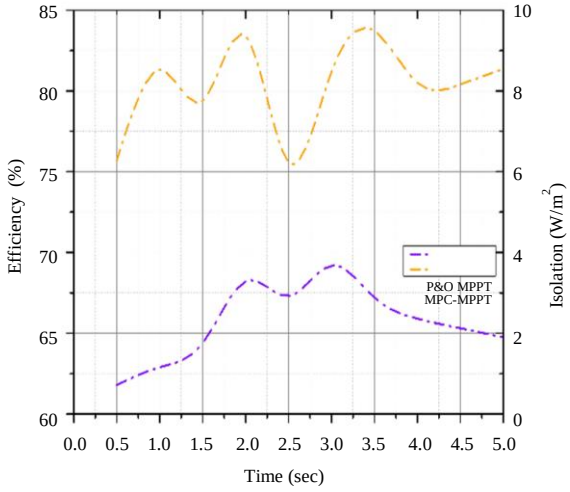

Fig. 16 Reactions of the system to the proposed strategy

The PV output closely matches the MPPT output and solar radiation level. However, when the insolation abruptly changes, PV power drops off significantly. Here's how to interpret it: The MPPT algorithm has a substantially longer sample time when compared to the system's sample time. As a result, the absorbed power from the PV will continue to be high until the MPPT sample occurs. The charging power has not experienced any variations in PV power. When the insolation is 50%, the PV generated is sufficient to power the EV and store the backup energy in the MPPT. At 50% insolation levels, the point is insufficient to charge the EV fully. This decrease in solar output will cause the MPPT to discharge. It should be considered that the MPPT has a higher degree of discharge power than the charging power. This event is due to internal MPPT inefficiencies. The charging and discharging procedures adjust as the amount of sunlight varies.

5. Conclusion

This work concerns the simulation-based design and testing of an MPPT approach using a flyback DC-DC converter, Perturb-and-Observe (P&O), and Model-Predictive Control (MPC). The MPPT technique based on the two algorithms is effective and speedy in simulations, maintaining the MPP at its ideal working point regardless of alterations in the surrounding temperature and light intensity. Additionally, it is demonstrated that the MPP working point's stable voltage operating was flawlessly accomplished.

The current study explains how to create a DC-DC flyback converter with maximum power point tracking capabilities and a solar Photovoltaic (PV) system. Both mathematical equations and operational states are provided. Benefits of the converter over competing topologies include lower peak power needs and greater magnetic core utilization.

Machine learning's significance in artificial intelligence is now well acknowledged. Machine learning uses training data analysis to optimize computational techniques. As more EVs hit the market, smart grid energy management must adjust to deal with new issues and opportunities. As real-world data experiments show, the two suggested strategies can significantly help lower operational costs and peak power usage compared to the two baselines. Its small appearance and fewer power components than conventional overlapping systems come from a single secondary winding and output diode.

The present investigation uses a bidirectional interleaved switched capacitor DC-DC converter to reduce voltage stress. Simulations and empirical data were used to validate the proposed topology, which assumes that all PV panels function according to an MPPT algorithm, proving its viability. The power converter architecture has proven effective for different solar radiation levels. The current study presents an improved MPPT approach that employs MPC to forecast mistakes in the upcoming collecting phase.

As a result, the switching signal can be altered beforehand. The results show that the MPC methodology makes MPP tracking possible much quicker than the P&O method. The central solar photovoltaic inverter generates useful power for such usage based on flyback design. Due to their low complexity, simple power flow management, and acceptable power quality during grid integration, flyback DC-DC converters are preferred.

References

[1] Mamta Agiwal, Abhishek Roy, and Navrati Saxena, "Next Generation 5G Wireless Networks: A Comprehensive Survey," *IEEE Communications Surveys and Tutorials*, vol. 18, no. 3, pp. 1617-1655, 2016. [CrossRef] [Google Scholar] [Publisher Link]

[2] Weijia Wang et al., "High-Performance Printable 2.4 GHz Graphene-Based Antenna Using Water-Transferring Technology," *Science and Technology of Advanced Materials*, vol. 20, no. 1, pp. 870-875, 2019. [CrossRef] [Google Scholar] [Publisher Link]

[3] Sumit Kumar et al., "Fifth Generation Antennas: A Comprehensive Review of Design and Performance Enhancement Techniques," *IEEE Access*, vol. 8, pp. 163568-163593, 2020. [CrossRef] [Google Scholar] [Publisher Link]

[4] Rongguo Song et al., "Wideband and Low Sidelobe Graphene Antenna Array for 5G Applications," *Science Bulletin*, vol. 66, no. 2, pp. 103-106, 2020. [CrossRef] [Google Scholar] [Publisher Link]

[5] Xinyao Zhou et al., "Graphene Printed Flexible and Conformal Array Antenna on Paper Substrate for 5.8 GHz Wireless Communications," *2020 14th European Conference on Antennas and Propagation (EuCAP)*, pp. 1-4, 2020. [CrossRef] [Google Scholar] [Publisher Link]

[6] Hao-Ran Zu et al., "Circularly Polarized Wearable Antenna with Low Profile and Low Specific Absorption Rate Using Highly Conductive Graphene Film," *EEE Antennas and Wireless Propagation Letters*, vol. 19, no. 12, pp. 2354-2358, 2020. [CrossRef] [Google Scholar] [Publisher Link]

[7] Wonbin Hong, "Solving the 5G Mobile Antenna Puzzle: Assessing Future Directions for the 5G Mobile Antenna Paradigm Shift," *IEEE Microwave Magazine*, vol. 18, no. 7, pp. 86-102, 2017. [CrossRef] [Google Scholar] [Publisher Link]

[8] Wei Hong et al., "Multibeam Antenna Technologies for 5G Wireless Communications," *IEEE Transactions on Antennas and Propagation*, vol. 65, no. 12, pp. 6231-6249, 2017. [CrossRef] [Google Scholar] [Publisher Link]

[9] Syeda Fizzah Jilani et al., "Millimeter-Wave Liquid Crystal Polymer Based Conformal Antenna Array for 5G Applications," *IEEE Antennas and Wireless Propagation Letters*, vol. 18, no. 1, pp. 84-88, 2019. [CrossRef] [Google Scholar] [Publisher Link]

[10] Chun-Xu Mao et al., "Planar Sub-Millimeter-Wave Array Antenna with Enhanced Gain and Reduced Sidelobes for 5G Broadcast Applications," *IEEE Transactions on Antennas and Propagation*, vol. 67, no. 1, pp. 160-168, 2019. [CrossRef] [Google Scholar] [Publisher Link]

[11] Lars Josefsson, and Patrik Persson, *Conformal Array Antenna Theory and Design*, IEEE Press Series on Electromagnetic Wave Theory, John Wiley and Sons, pp. 1-83, 2006. [Google Scholar] [Publisher Link]

[12] Wael Ali et al., "Planar Dual-Band 27/39 GHz Millimeter-Wave MIMO Antenna for 5G Applications," *Microsystem Technologies*, vol. 27, pp. 283-292, 2021. [CrossRef] [Google Scholar] [Publisher Link]

[13] Oluseun Oyeleke Wikiman et al., "PIFA Antenna Design for MmWave Body Centric 5G Communication Applications," *SSRG International Journal of Electronics and Communication Engineering*, vol. 6, no. 4, pp. 6-10, 2019. [CrossRef] [Google Scholar] [Publisher Link]

[14] Thomas E. Morton, and Krishna M. Pasala, "Pattern Synthesis of Conformal Arrays for Airborne Vehicles," *2004 IEEE Aerospace Conference Proceedings*, vol. 2, pp. 1030-1039, 2004. [CrossRef] [Google Scholar] [Publisher Link]

[15] Jiazhi Dong et al., "A Research on Airborne Conformal Array with High Gain and Low SLL," *2014 International Conference on Computational Intelligence and Communication Networks*, pp. 334-338, 2014. [CrossRef] [Google Scholar] [Publisher Link]

[16] Yeqin Huang, and Shieh T. Hsieh, "Radiation of Conformal Slot Arrays on Perfectly Conducting Super-Spheroid," *2005 IEEE International Symposium on Microwave, Antenna, Propagation and EMC Technologies for Wireless Communications*, vol. 1, pp. 601-604, 2005. [CrossRef] [Google Scholar] [Publisher Link]

[17] L. Zou, J. Lasenby, and Z. He, "Beamforming with Distortion Less Co-Polarization for Conformal Arrays Based on Geometric Algebra," *IET Radar, Sonar and Navigation*, vol. 5, no. 8, pp. 842-853, 2011. [CrossRef] [Google Scholar] [Publisher Link]

[18] K.M. Tsui, and S.C. Chan, "Pattern Synthesis of Narrowband Conformal Arrays Using Iterative Second-Order Cone Programming," *IEEE Transactions on Antennas and Propagation*, vol. 58, no. 6, pp. 1959-1970, 2010. [CrossRef] [Google Scholar] [Publisher Link]

[19] Yan-Ying Bai et al., "A Hybrid IWO/PSO Algorithm for Pattern Synthesis of Conformal Phased Arrays," *IEEE Transactions on Antennas and Propagation*, vol. 61, no. 4, pp. 2382-2332, 2013. [CrossRef] [Google Scholar] [Publisher Link]

[20] Massimiliano Comisso, and Roberto Vescovo, "3D Power Synthesis with Reduction of Near-Field and Dynamic Range Ratio for Conformal Antenna Arrays," *IEEE Transactions on Antennas and Propagation*, vol. 59, no. 4, pp. 1164-1174, 2011. [CrossRef] [Google Scholar] [Publisher Link]

[21] Srabonty Soily, Rezaul Karim Mazumder, and Khaleda Ali, "Design and Simulation of Two Conformal Arrays with Dual Patch and Quadruple Patch Antenna Elements," *2015 IEEE Conference on Antenna Measurements and Applications (CAMA)*, pp. 1-3, 2015. [CrossRef] [Google Scholar] [Publisher Link]

[22] M. Comisso, and Roberto Vescovo, "Fast 3D Pattern Synthesis for Conformal Antenna Arrays with Cross-Polarization Reduction," *2010 IEEE Antennas and Propagation Society International Symposium*, pp. 1-4, 2010. [CrossRef] [Google Scholar] [Publisher Link]

[23] Meysam Rasekh, and Saeid R. Seydnejad, "Design of an Adaptive Wideband Beamforming Algorithm for Conformal Arrays," *IEEE Communications Letters*, vol. 18, no. 11, pp. 1955-1958, 2014 [CrossRef] [Google Scholar] [Publisher Link]

[24] K. Woelders, and J. Granholm, "Cross-Polarization and Sidelobe Suppression in Dual Linear Polarization Antenna Arrays," *IEEE Transactions on Antennas and Propagation*, vol. 45, no. 12, pp. 1727-1740, 1997. [CrossRef] [Google Scholar] [Publisher Link]

[25] Harmen Schippers et al., "Conformal Phased Array with Beam Forming for Airborne Satellite Communication," *2008 International ITG Workshop on Smart Antennas*, pp. 334-350, 2008. [CrossRef] [Google Scholar] [Publisher Link]

[26] Peter Knott, "Design of a Triple Patch Antenna Element for Double Curved Conformal Antenna Arrays," *2006 First European Conference on Antennas and Propagation*, pp. 1-4, 2006. [CrossRef] [Google Scholar] [Publisher Link]

[27] Ziheng Ding et al., "High Aperture Efficiency Arced Conformal Array with Phasor Beam Steering Antenna," *IEEE Transactions on Antennas and Propagation*, vol. 71, no. 1, pp. 596-605, 2022. [CrossRef] [Google Scholar] [Publisher Link]

[28] Fujun Xu et al., "Performance and Impact Damage of a Three Dimensionally Integrated Microstrip Feeding Antenna Structure," *Composite Structures*, vol. 93, no. 1, pp. 193-197, 2010. [CrossRef] [Google Scholar] [Publisher Link]

[29] Lan Yao et al., "Fabrication and Impact Performance of Three-Dimensionally Integrated Microstrip Antennas with Microstrip and Coaxial Feeding," *Smart Materials and Structures*, vol. 18, no. 9, 2009. [CrossRef] [Google Scholar] [Publisher Link]

[30] Brajlata Chauhan et al., "Cylindrical Conformal Antenna Arrays Theory for Military Aircraft Antenna," *2020 IEEE International Conference on Computing, Power and Communication Technologies (GUCON)*, pp. 77-82, 2020. [CrossRef] [Google Scholar] [Publisher Link]

[31] Bahare Mohamadzade et al., "Recent Developments and State of the Art in Flexible and Conformal Reconfigurable Antennas," *Electronics*, vol. 9, no. 9, pp. 1-26, 2020. [CrossRef] [Google Scholar] [Publisher Link]

[32] Garima D. Bhatnagar et al., "Design of Broadband Circular Patch Microstrip Antenna with Diamond Shape Slot," *Indian Journal of Radio and Space Physics*, vol. 40, pp. 275-281, 2011. [Google Scholar] [Publisher Link]

[33] Neng-Wu Liu et al., "A Low-Profile Aperture-Coupled Microstrip Antenna with Enhanced Bandwidth Under Dual Resonance," *IEEE Transactions on Antennas and Propagation*, vol. 65, no. 3, pp. 1055-1062, 2017. [CrossRef] [Google Scholar] [Publisher Link]

[34] Ling Sun et al., "Two-Port Pattern Diversity Antenna for 3G and 4G MIMO Indoor Applications," *IEEE Antennas and Wireless Propagation Letters*, vol. 13, pp. 1573-1576, 2014. [CrossRef] [Google Scholar] [Publisher Link]

[35] Wei Lin, Richard W. Ziolkowski, and Hang Wong, "Pattern Reconfigurable Techniques for LP and CP Antennas with the Broadside and Conical Beams," *12th European Conference on Antennas and Propagation (EuCAP 2018)*, pp. 1-4, 2018. [CrossRef] [Google Scholar] [Publisher Link]